Carrier generation in photoconductive poly(*N*-vinylcarbazole) as revealed by multifrequency time-resolved ESR

Tadaaki Ikoma,* Kimio Akiyama, and Shozo Tero-Kubota
Institute of Multidisciplinary Research for Advanced Materials, Tohoku University, Katahira 2-1–1, Aokaku, Sendai 980-8577, Japan
(Received 16 October 2004; revised manuscript received 2 February 2005; published 26 May 2005)

Using the multifrequency time-resolved electron-spin-resonance (TRESR) method, we have investigated the carrier-generation dynamics in a photoconductive film sample of poly(*N*-vinylcarbazole). The TRESR spectra, due to spin-polarized geminate electron-hole (e-h) pairs captured in deep-trap sites, were observed at several fields that were achieved using microwaves with different frequencies. The spectra detected at room temperature were interpreted in terms of the ST_0 polarization in trapped e-h pairs and the ST_+ polarization induced in canonical e-h pairs. The spectral simulation clarified the distribution of e-h separation distance (r) and the r-dependent recombination of the trapped pairs. The initial spatial distribution of the trapped e-h pairs exponentially decreased with an increase in r. There is no large population of long-distant e-h pairs with $r > 1.5$ nm. Based on the appearance of the ST_+ polarization in the long-distant pairs that is generated in middle-distant pairs and the initial exponential distribution of the trapped pairs, it was concluded that stepwise hole hops rather than a long-range hole jump represent the proper dynamics of the geminate pair in the charge-separation process. The r-dependent recombination rate suggests a single-step tunneling recombination of the trapped pairs.

DOI: 10.1103/PhysRevB.71.195206 PACS number(s): 72.20.Jv, 72.25.−b, 36.20.−r, 76.30.−v

I. INTRODUCTION

At least two processes can be distinguished in the photoconduction in sensitized amorphous solids consisting of aromatic neutral molecules. In the first process, a geminate distant electron-hole (e-h) pair is somehow created after the light quantum absorption, and it produces carriers through a dissociation step, depending on an external electric field. The field dependence in this carrier generation is understood by the Onsager theory.[1,2] The second process is the transportation of carriers generated from the geminate e-h pair, which finally results in the conduction of the aromatic organic materials. Polymeric solids of tertiary aromatic amines are the most widely used as photoreceptors and hole transport layers. An amorphous film of the poly(*N*-vinylcarbazole) (PVCz) shown in Fig. 1 is one of the best hole-photoconductive molecular solids that has been extensively investigated so far.[3,4] It is well known that doping an electron acceptor such as 2,4,7-trinitro-9-fluorenone or 1,2,4,5-tetracyanobenzene (TCNB) in the solids of carbazolyl (Cz) chromophers enhances the photoconductivity substantially. Regarding the initial charge separation for the long-distant e-h pair in the carrier generation of the acceptor-doped PVCz film, two different kinds of hole dynamics are proposed. One is a long-range hole jump up to a few nanometers, assuming thermalization,[5–10] autoionization,[11] tunneling,[12] or a coherent motion of the surrounding molecules.[13] Another one is stepwise hole hops among the neighboring aromatic molecules.[14–18] To clarify the initial hole dynamics on a nanoscale, it is desired to observe the geminate e-h pair directly.

Electron spin resonance (ESR) is a unique method that can determine the nanoscale structure of the e-h pair accurately,[19–22] if the pair has unpaired electrons. In the case of a magnetic-field modulation technique for sensitivity enhancement in a conventional ESR method, however, time resolution is not fast enough to detect transient paramagnetic pairs with lifetimes of less than 1 ms. In principle, the direct detection system in which field modulation is not employed makes it possible to follow the transients from a subnanosecond region. Recently, by using this time-resolved ESR (TRESR) method, we succeeded in detecting the geminate e-h pair in a TCNB-doped PVCz film.[23] The population among the electron-spin states of the observed e-h pair differed from the Boltzmann distribution at ambient temperature. Such a nonthermalized population of the electron-spin states is called the electron-spin polarization. Generally, electron-spin polarization is created by intramolecular relaxation from electronically excited states and dynamic magnetic interaction between paramagnetic species. Therefore, it is closely related to the kinetics that the e-h pair has undergone before becoming itself as well as the structure of the e-h pair.[24–29] In this paper, we carried out detailed experiments using the multifrequency TRESR method and could make a reliable assignment of the spin-polarized e-h pair. Quantitative analysis of the spin-polarized spectrum using the stochastic Liouville equations (SLE) allowed us to rigorously discuss the hole dynamics in the carrier generation and the recombination of the trapped e-h pair.

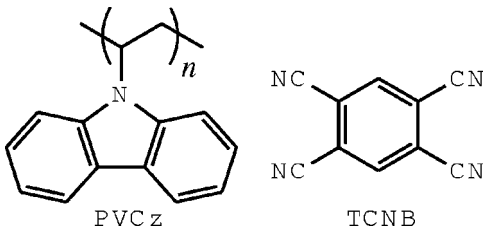

FIG. 1. Molecular structures of poly (*N*-vinylcarbazole) (PVCz) and 1,2,4,5-tetracyanobenzene (TCNB).

II. EXPERIMENTAL SECTION

PVCz with a mean unit number of around 5.7×10^3 (Aldrich) was purified before use by reprecipitation with toluene and ethanol. TCNB (Tokyo Kasei) recrystallized from ethanol was employed. For ESR measurements, TCNB-doped PVCz amorphous films with a thickness of less than 50 μm were prepared in quartz tubes by casting a toluene solution in which PVCz and TCNB were mixed at a monomer molar ratio of 98:2. The amorphous films in the tubes were placed under vacuum at $\sim10^{-2}$ Pa for 24 h to remove the remaining toluene, oxygen, and other volatile substances. The TCNB-doped film had a broad absorption band in the wavelength region from 380 nm to 730 nm, due to the charge-transfer (CT) complex between TCNB and contact Cz, in which the charges are partly separated. The absorbance around the peak position of the CT band of the prepared film samples was about 0.05. The model compounds of electrons and holes in the TCNB-doped PVCz were respectively prepared by the contact reduction of the TCNB with sodium metal in a methyltetrahydrofuran solvent under vacuum and by the oxidation of PVCz dissolved in concentrated sulfuric acid.

TRESR measurements were performed using *X*-band (9.3 GHz), *Q*-band (34.0 GHz), and *W*-band (94.1 GHz) spectrometers (Varian E-109E, Bruker ESP300, Bruker ELEXES E600) without magnetic-field modulations. To excite the CT complex selectively, Nd^{3+}:YAG lasers (Quanta-Ray, GCR-14, and GCR-150, 532 nm) and an OPO laser (Quanta-Ray, MOPO-710, 590 nm) were used as the light sources. The power density and full width at half maximum of the pulse lasers were less than 10 mJ $pulse^{-1}$ cm^{-2} and approximately 20 ns, respectively. To obtain random orientational ESR spectra, the linearly polarized light from the laser was passed through a quartz depolarizer located before the sample position. For the magnetophotoselection experiments, the plane of the polarized light was controlled using a $\lambda/4$ plate and a Gran laser prism located before the sample position. The amorphous samples were irradiated in the microwave cavities of a rectangular TE_{102} or cylindrical TE_{011} mode. The ESR signals from a broadband preamplifier were fed into boxcar averagers (EG&G 4121B and 162) or fast digital oscilloscopes (LeCroy 9450A, Tektroninx 2440, and Bruker SpecJet). Several hundred transients were recorded and averaged to improve the signal-to-noise (S/N) ratio. A helium flow system (Oxford ESR900) was used for measurements at low temperatures.

III. RESULTS

A. Transient ESR spectra

Figure 2 shows the transient *X*-band TRESR spectra observed when the CT complex in the TCNB-doped PVCz solid was directly excited to form a contact e-h pair using the pulse laser with a wavelength of 532 nm at 293 K. At 300 ns after the laser flash, spin-polarized signals were detected over a relatively wide range from 0.326 to 0.338 T [Fig. 2(a)]. To assign the observed transient paramagnetic species, we measured separately the conventional steady-state ESR spectra of model compounds for the electrons and holes in this polymeric solid, which were respectively the TCNB anion and the PVCz cation in rigid glassy solvents. The spectra for both free ions possessed a peak at a magnetic field corresponding to $g=2.0028$. Their spectral widths were nearly determined by individual intramolecular hyperfine interactions. The central field of the transient ESR spectrum for the TCNB-doped PVCz film was in agreement with $g=2.0028$, which indicated that the transient species were associated with the $TCNB^-$ and $PVCz^+$ radicals. However, the spectral width of the transient signal in the film sample was much broader than that of the component-free ions. The breadth of the TRESR spectrum at 300 ns indicated that the transient signal was attributed to the e-h pair rather than to the free ions, the so-called carriers, because the intermolecular magnetic interactions of the exchange and dipolar interactions between the electron and hole could broaden the spectrum. The spectrum of the e-h pair basically had a smooth structure, but there were two humps at 0.327 and 0.337 T.

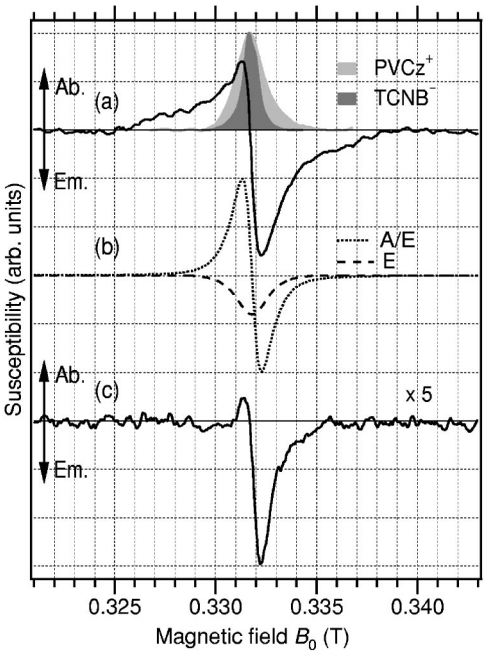

FIG. 2. *X*-band TRESR spectra of the trapped geminate e-h pair in a TCNB-doped PVCz film observed at 300 ns (a) and 4 μs (c) after pulse excitation of the CT band at 293 K. (b) The broken lines schematically illustrate the spectral patterns for the multiplet A/E—and net E—polarizations. The gray-colored signals in (a) are steady-state ESR spectra of a $PVCz^+$ radical in conc. H_2SO_4 and a $TCNB^-$ radical in 2-methyl tetrahydrofuran at 8 K.

The spin-thermalized particles had net absorptive ESR signals, but the spectrum due to the e-h pair observed at 300 ns showed an unusual phase of enhanced absorption (A) in the low-field half and emission (E) in the high-field half. The signal intensity of E polarization in the high field was stronger than that of A polarization in the low field, which is called A/E^* polarization. The observed A/E^* polarization was interpreted in terms of multiplet A/E polarization having a point symmetry about the center of the spectrum and net E polarization having total emission over the whole spectral range [Fig. 2(b)].[30] The multiplet A/E polarization was safely assigned to a spin polarization by a spin-correlated

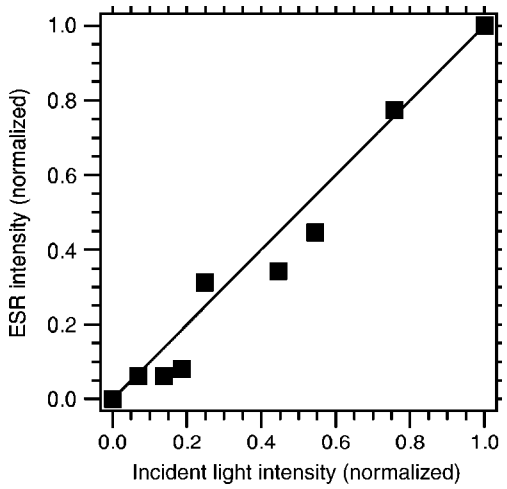

FIG. 3. Incident laser-power dependence of the intensity of the TRESR spectrum for trapped e-h pairs detected at 300 ns at 293 K.

radical-pair mechanism in which a coherent spin conversion took place between the singlet (S) and middle triplet (T_0) sublevels. Such a multiplet polarization was mainly caused by the difference in mutual hyperfine interactions between the electron and hole. Multiplet polarization was hardly expected during the hole hops, because the sign of nuclear-spin sublevels of the hole may have changed due to the hopping. We could say, therefore, that the e-h pairs detected at 300 ns were the pairs that were not undergoing hole hops anymore. It was reasonable that the hole had been captured in trap sites in which the energy depth was deeper than the thermal energy of $\sim$25 meV at room temperature. As far as the origin of the net E polarization was concerned, although there were several possibilities at this stage, it was attributable to ST_+ polarization, based on the magnetic-field dependence of the spin polarization described later.

The spin-polarized spectrum decreased in intensity with the delay time. Also, it was noteworthy that the spectral shape gradually changed with time. The signals separated by more than 6 mT in the spectrum disappeared at 4 μs, as shown in Fig. 2(c), while the signals in the central region that were comparable to the linewidth of the free ions were still observed at a few tens of μs. At a later time, the contribution of the net E polarization became stronger in comparison with the multiplet A/E polarization. Hence, the observed spectrum of the trapped e-h pairs seemed to be roughly divided into two categories of a short-lived broad component with multiplet A/E-plus weak net E-polarizations and a long-lived sharp component with A/E-plus strong E-polarizations. The different time dependence between these components suggested a single-step recombination process depending on the e-h separation distance rather than the multistep hole hops.[31–39]

The intensity of the TRESR signal increased with the incident power of the laser excitation. A plot of the ESR intensity versus the laser power is given in Fig. 3. The linear laser-power dependence with the unit of slope indicates that the observed e-h pair was created through a one-photon process. On the other hand, the decay behavior of the ESR spectrum was not influenced by the incident laser power. Because

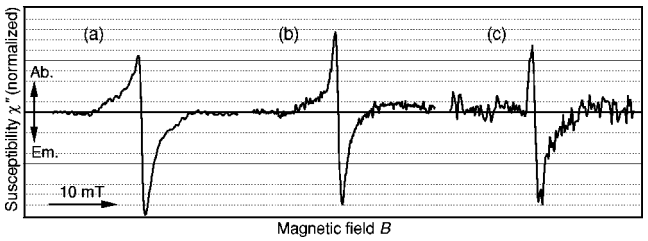

FIG. 4. The TRESR spectra at 300 ns for the trapped e-h pairs measured at 0.33 T (a), 1.21 T (b), and 3.36 T (c). These spectra were measured at 293 K using microwaves with frequencies of 9.299, 33.999, and 94.141 GHz, respectively.

the recombination within free e-h pairs should be accelerated by an increase in laser power, no power dependence of the signal decay shows that the observed e-h pairs decay through geminate recombination.

Irradiation with a linearly polarized light preferentially excited the CT complexes such that their transition moment in the CT band was along the polarized direction of the light. Hence, the linearly polarized light enabled an angle-selection experiment in the randomly oriented sample to be performed. The ESR spectrum was broadened by anisotropy because of the dipolar interaction, therefore, the shape of the spectrum might have been distorted by the angle-selection experiment,[40–44] as long as the e-h pair retained the initial orientation of the CT complex. However, excitation with the polarized light did not have any influence on the spectral shape. No effect of the angle-selection experiments could be interpreted in terms of the loss of memory of the initial orientation of the e-h pair due to hole migration by multistep hole hops or a long-range hole jump.

B. Magnetic-field dependence of spin polarization

Figure 4 shows the TRESR spectra of the trapped e-h pairs in the PVCz film observed at 300 ns using 9.3, 34, and 94 GHz microwaves, the measurements of which were carried out around the fields of 0.33, 1.21, and 3.36 T, respectively. The multiplet A/E polarization due to the ST_0 mixing was observed in all fields, while clear net E polarization was not seen at 1.21 T and 3.36 T. The field dependence of the net E polarization led to the conclusion that the spin dynamics for the net E polarization of the trapped e-h pairs took place at a specific magnetic field. So far, several mechanisms have been established for dynamic spin polarizations giving a net E polarization, for example, the Δg effect, the triplet mechanism (TM), the spin-orbit coupling mechanism (SOCM), and ST_+ mixing. The observed field dependence of the net E polarization excludes the Δg effect, because the Δg polarization increases with an increase in the field. Because the e-h pairs arose from the singlet state under the experimental conditions of the selective excitation of the CT complex, the TM polarization that arises from the dynamics of local excited triplet states is not feasible. The SOCM polarization that is due to the spin sublevel selective charge transfer induced by heavy atoms[45–50] can also be neglected in the case of the organic molecular system in which neither halogens nor metals were included. The appearance of the net E

polarization at a specific field only is consistent with the spin polarization, due to the ST_+ mixing within the e-h pair. The magnetic field where the Zeeman energy was comparable to the exchange interaction within the e-h pair gave rise to the energy proximity between the S state and either the top (T_+) or bottom (T_-) triplet sublevel, depending on the sign for the exchange-interaction constant (J). This energy proximity provided an opportunity of the net E polarization of ST_+ mixing or the net A polarization of ST_- mixing.[51–53] The E polarization of the trapped e-h pairs in the PVCz film observed around 0.34 T indicates ST_+ mixing in the e-h pairs with a positive J value near 0.17 (=0.34/2)T, which may not be the case when the e-h separation distance is long.

IV. DISCUSSION

A. ST_0 polarization

The trapped e-h pairs observed in the TCNB-doped PVCz film sample mainly had multiplet spin polarization due to the ST_0 mixing within the pair. In order to obtain information on the structure of the trapped e-h pair, we performed simulations of the spectrum. The spin Hamiltonian for the e-h pair ($\boldsymbol{H}_{eh}$) can be written in angular frequency units,

$$\boldsymbol{H}_{eh} = \omega_e S_{ez} + \omega_h S_{hz} - J\left(\boldsymbol{S}_e\boldsymbol{S}_h - \frac{1}{2}\right) + D\left(\cos^2\theta - \frac{1}{3}\right)(3S_{ez}S_{hz} - \boldsymbol{S}_e\boldsymbol{S}_h), \tag{1}$$

$$\omega_i = \frac{g_i\mu_B B}{\hbar} + \sum_j A_j^i M_j^i, \quad i = e,h. \tag{2}$$

ω_e and ω_h in the first two terms are determined by the Zeeman and hyperfine interactions of the electron and hole, respectively. The g factor and Bohr magneton are represented by g and μ_B, respectively. B is the applied magnetic field. A_j^i and M_j^i are the hyperfine coupling constant and magnetic quantum number of nucleus j, respectively. S_{ez} and S_{hz} are the z components of the electron spin operators $\boldsymbol{S}_e$ and $\boldsymbol{S}_h$, respectively, with $\boldsymbol{S}_i=(S_{ix},S_{iy},S_{iz})$, $i=e,h$. J and D in the last two terms are the constants for the isotropic exchange and anisotropic dipolar interactions between the electron and hole. The dipolar interaction is assumed to be axial for simplicity and depends on the orientation of θ that is the angle between the vector connecting the two charged particles and the magnetic field B. It is equivalent to the colatitude in a spherical polar coordinate. The e-h pair had four sublevels of electron spins as shown in Fig. 5.[21] The triplet sublevels of the e-h pair were split into three, T_+, T_0, and T_-, by the Zeeman and dipolar interactions. The energy location of the S state of the e-h pair relative to the triplet sublevels was nearly determined by the exchange interaction. In the case of e-h pairs having a relatively long separation distance, the J value is much smaller than the splittings among the triplet sublevels. Because the S state energetically existed near the T_0 state, an effective interaction with the T_0 state resulted in the new mixed states denoted by $|2\rangle$ and $|3\rangle$. Consequently, the population transfer between these states occurred according to the difference between ω_e and ω_h which corresponds

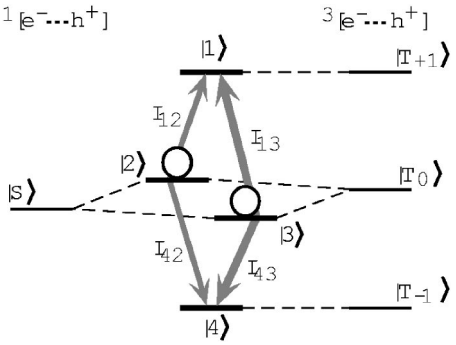

FIG. 5. Energy scheme of the spin states for a singlet-born e-h pair under a magnetic field and four allowed resonances with the microwave. The circles and arrows denote populations and transitions, respectively.

to the ESR frequency difference between the electron and hole. On the other hand, the T_+ and T_- states did not mix with the S state due to the ω difference, because of the large energy separation. Thus the $|1\rangle$ and $|4\rangle$ states retained the character of the T_+ and T_- states, respectively. In the case of singlet-born pairs, the resonances from the $|2\rangle$ and $|3\rangle$ states to the $|1\rangle$ state (I_{12} and I_{13}) produced the A-phase ESR signals. The E-phase signals arose from the resonances from the $|2\rangle$ and $|3\rangle$ states to the $|4\rangle$ state (I_{42} and I_{43}).

The eigenvalues of the spin Hamiltonian that were reduced to the resonance fields in the ESR spectrum of the e-h pair are obtained by diagonalization with a basis set of $|S\rangle, |T_+\rangle, |T_0\rangle$, and $|T_-\rangle$. It is also necessary to determine the spin populations in the S and T_0 states to calculate the multiplet-polarized spectrum. Under the high-field approximation, the time evolution of the density operator $[\rho(t)]$ in the two-level system of the S and T_0 states was analytically derived by the SLE comprised of the above spin Hamiltonian for a singlet-born radical pair.[54] From the density-matrix elements, therefore, the ESR signal intensities are calculated as follows:[55]

$$I_{12} = -I_{42} = \frac{1}{2}[c^2\rho_{SS} + s^2\rho_{T_0T_0} + cs(\rho_{ST} + \rho_{TS})]s^2, \tag{3}$$

$$I_{13} = -I_{43} = \frac{1}{2}[s^2\rho_{SS} + c^2\rho_{T_0T_0} - cs(\rho_{ST} + \rho_{TS})]c^2, \tag{4}$$

where

$$c = \cos\psi, \quad s = \sin\psi; \tag{5}$$

$$\tan 2\psi = \frac{Q}{j}, \quad Q = \frac{\omega_e - \omega_h}{2}, \quad j = J + \frac{D}{2}\left(\cos\theta - \frac{1}{3}\right). \tag{6}$$

Here we define the resonance line-shape function of $f(\boldsymbol{H}_{eh}, I_{12}, I_{13}, I_{42}, I_{43})$ given by the calculations, using the equations mentioned above. The transient ESR spectrum at a time t for the ST_0-polarized e-h pairs (S_{ran}), which is randomly oriented in the amorphous film under the external magnetic field, is obtained by integrating f with respect to the spherical polar angles.

TABLE I. Magnetic interaction and kinetic constants used for the simulations and parameters obtained by simulations.

electron		hole		distance		exchange		recombination		rate constants		
g_{av}	ω_{hfi}(MHz)	g_{av}	ω_{hfi}(MHz)	r_1(nm)	r_e(nm)[a]	J_1(MHz)[a]	α(nm^{-1})	k_1(s^{-1})[a]	β(nm^{-1})	k_H(s^{-1})	k_f(s^{-1})	k_t(s^{-1})[a]
2.0028	21.2	2.0028	41.0	0.5	0.21	−200	10	1×10^7	10	4.5×10^8	7.0×10^7	1×10^7

[a]These parameters were optimized in simulations of the TRESR spectra and the separation-distance distribution of trapped e-h pairs.

$$S_{ran}(t,\omega_e,\omega_h,J,D)=\int_0^{2\pi}\int_0^{\pi} f(\boldsymbol{H}_{eh},I_{12},I_{13},I_{42},I_{43})\sin\theta d\theta d\varphi$$
$$=2\pi\int_0^{\pi} f(\boldsymbol{H}_{eh},I_{12},I_{13},I_{42},I_{43})\sin\theta d\theta. \quad (7)$$

φ is the azimuth around the direction of B.

The calculation of a concrete ST_0-polarized spectrum with the S_{ran} function requires the magnetic variables of ω_e,ω_h,J, and D in the spin Hamiltonian and the functions of the ESR signal intensities. The g and hyperfine tensors of the electron and hole were not estimated precisely because of the structureless spectra of the $TCNB^-$ anion and $PVCz^+$ cation. However, the individual spectra for these radicals were well fitted by the normalized Gaussian functions, having $g_{av}=2.0028$, $\Delta\omega_{hfi}=21.2$ MHz and $g_{av}=2.0028$, $\Delta\omega_{hfi}=41.0$ MHz, respectively (Table I). g_{av} corresponds to the central position and $\Delta\omega_{hfi}$ means the full width at half maximum in the Gaussian. These approximated constants in the individual interactions were employed for the simulations described later. On the other hand, the J and D constants in the interspin interaction between the electron and hole depend on the e-h separation distance (r). The r dependence for the exchange interaction due to the direct overlap between the singly occupied orbitals is expressed by an exponential function of

$$J(r;J_1,\alpha)=J_1\exp[-\alpha(r-r_1)]. \quad (8)$$

The contact distance between the electron and hole r_1 can be replaced by 0.5 nm, according to the molecular sizes of the TCNB and Cz monomer unit. J_1 and α are characteristic parameters of the general exponential function. These parameters have substantial variations in many literature sources.[56–61] Their variations may arise from the mechanism difference in the exchange interaction in ionic systems.[62–66] Because the present photoconductive polymer is also an ionic system, it is reasonable to assume an α value of 1.0×10^1 nm^{-1} and let J_1 be a parameter to be optimized in the simulation. Within the point-dipole approximation,[67] the dipolar interaction can be written as

$$D(r)=-\frac{3}{2}\frac{(g\mu_B)^2}{r^3}, \quad (9)$$

where g is the average g factor of the pair. The D value as well as the J value decreases monotonously with an increase in r. From the consideration above, consequently, it is clear that only J_1 and r among many variables in S_{ran} are simulation parameters.

Before discussing the simulated spectrum for the trapped e-h pairs in the PVCz film sample, it is instructive to consider what the ST_0-polarized ESR spectrum looks like in J and D spaces using the individual g and hyperfine constants of the electron and hole in TCNB-doped PVCz. Figure 6 depicts two-dimensional plots of the simulated TRESR spectrum at $t=300$ ns, calculated using various J or D values. Assuming the D value to be zero, two lines with an A/E phase separated by $4|J|$ can be seen in the negative J space [Fig. 6(a)]. These two lines are attributed to the transitions of I_{13} and I_{43}. In the case of $D=0$ MHz, the absorptive I_{12} and emissive I_{42} transitions are located in the central field of the spectrum, and therefore almost cancel each other. When the J value approaches zero, the two outer lines of I_{13} and I_{43} shift into the center of the spectrum. Their signal intensity increases due to the increase in the transition probability of I_{13} and I_{43}, originating from the increase in the T_0 character in the $|3\rangle$ level, but finally becoming zero because of complete overlapping at $J=0$ MHz. In the negative D region with $J=0$ MHz [Fig. 6(b)], the calculated spectrum shows a similar A/E polarization, but it has a slightly broader shape than that in the case of the J space. The anisotropy of the dipolar interaction, which is different from the exchange interaction, induces the broad shape and some structures around the central field. The decrease in the signal intensity with the increase in the $|D|$ value also arises mainly from the uniaxially broadening of the line shape. The splitting between the outer signals is equal to $|D|$. On the other hand, the J and D dependences of the spin-polarized spectrum become complex when using a nonzero D or J value [Figs. 6(c) and 6(d)]. The splitting by $|D|$ and $4|J|$ can be seen at the zero position in the J and D spaces, respectively. The signals not only shift to the outer sides, but also increase in intensity with an increase in the J or D variable. The constructive sharpening and overlapping of the resonance lines give rise to the growth in signal intensity, which reaches a maximum at the position of $|D|=6|J|$. In the region beyond the maximized position in the parameter spaces ($D\leqslant 6J$, $J\leqslant D/6$), the spectrum becomes broader and decreases in intensity again.

In real space, both the J and D parameters should simultaneously vary with the e-h separation distance. Figure 7(a) shows the distance dependence of the J and D values calculated using Eq. (8) with substituted $J_1=-2.0\times10^2$ MHz and Eq. (9), respectively. The J value rapidly diminishes with an increase in the r distance, while the D value is effective even over a rather long distance. Based on these r dependences of the interspin-interaction parameters, we calculated the r variation of the ST_0-polarized spectrum for the singlet-born e-h pair as shown in Fig. 7(b). In a distance shorter than 0.6 nm where both the exchange and dipolar interactions are substantially large, we can see very weak broad signals split

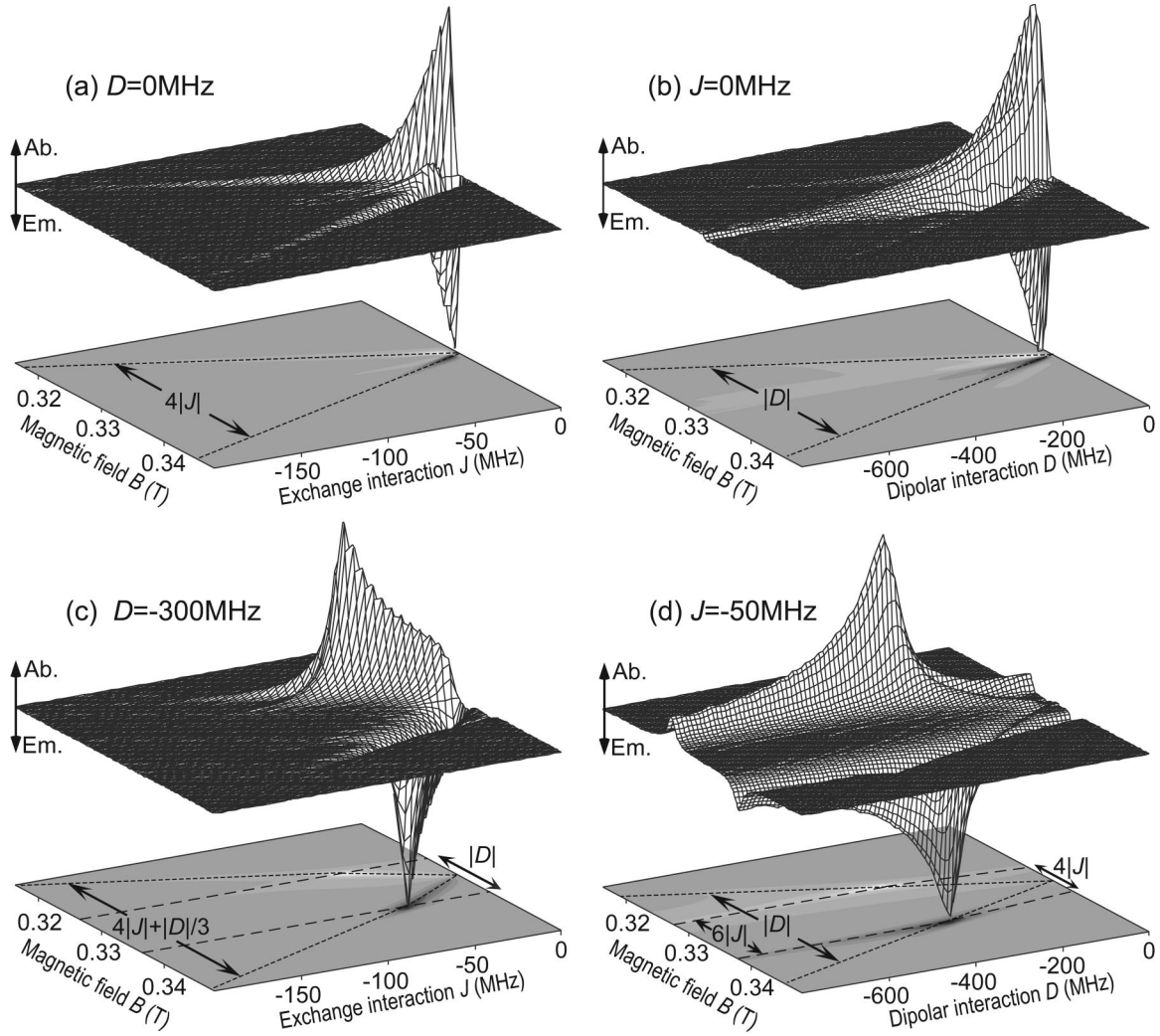

FIG. 6. Exchange and dipolar interaction dependences of the *X*-band spectrum calculated for the trapped e-h pair in the TCNB-doped PVCz film. These simulation spectra were calculated using the SLE with the parameters of $D=0$ MHz (a), $J=0$ MHz (b), $D=-300$ MHz (c), and $J=-50$ MHz (d). The magnetic constants of $TCNB^-$ ($g_{av}=2.0028$ and $\Delta\omega_{hfi}=21.2$ MHz) and $PVCz^+$ ($g_{av}=2.0028$ and $\Delta\omega_{hfi}=41.0$ MHz) were used to calculate the simulation spectra.

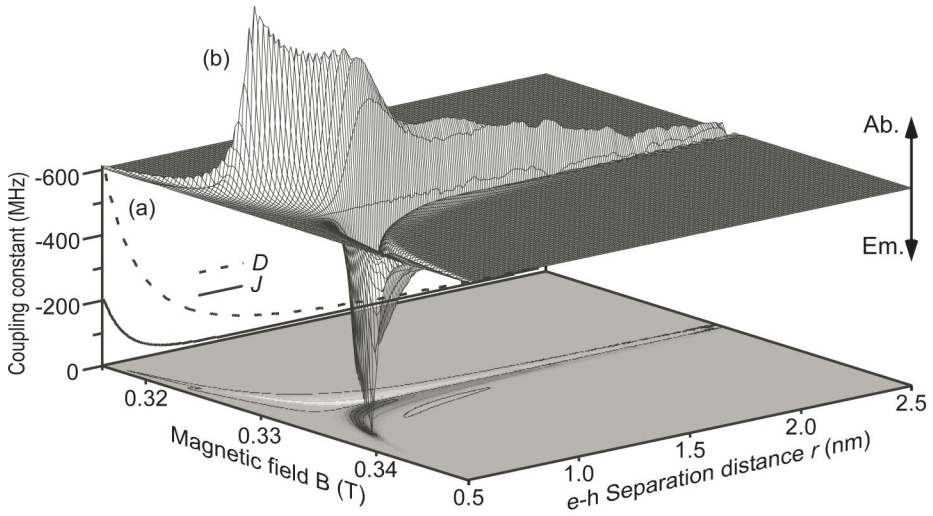

FIG. 7. Separation-distance dependence of the *X*-band spectrum calculated for the trapped e-h pair in the TCNB-doped PVCz film. The parameters in the *r*-dependent function of *J* used in the simulation are $J_1=-2.0\times10^2$ MHz, $\alpha=1.0\times10^1$ nm^{-1}, and $r_1=0.5$ nm. The other constants used in the calculation are the same as those in Fig. 6.

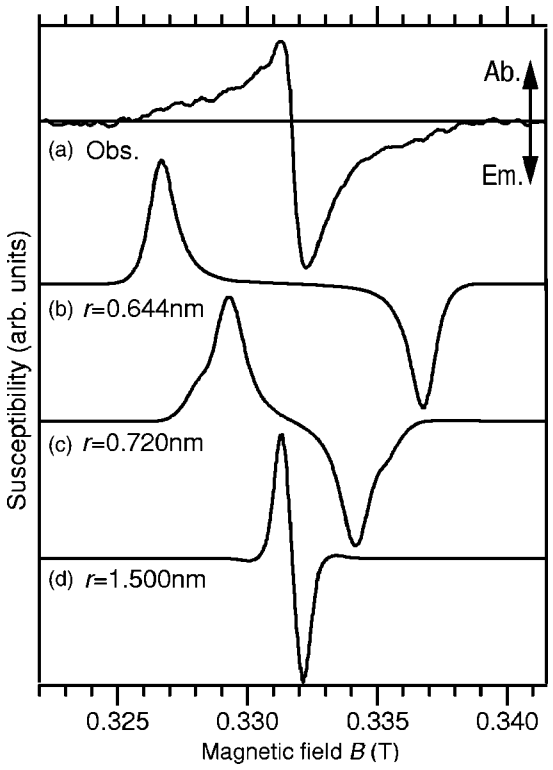

FIG. 8. *X*-band ESR spectra for the trapped e-h pair in the TCNB-doped PVCz film observed at 300 ns (a) and calculated using a series of constants estimated at $r=0.644$ (b) and 0.720 and 1.500 nm (d). The parameters employed for the calculations are the same as those in Fig. 7.

by a wide-field separation. Over 0.6 nm, the calculated spectrum drastically decreases in splitting because of the rapid reduction of the J value and dramatically enhances in intensity due to the constructive effect among the four resonance lines. The signal intensity is the largest around 0.64 nm where the condition of $|D|=6|J|$ is fulfilled. Beyond the maximized distance, the spectrum decreases in intensity due to the destructive overlap between the A phase and E phase lines due to the rapid reduction of the J value. At more than 0.90 nm where the J value is negligible but the D value is still effective, the splitting of the A/E-polarized spectrum becomes even smaller gradually, which reflects the slow decay of the dipolar interaction. The slow decrease beyond approximately 1.3 nm is interpreted in terms of the destructive overlapping of the resonance lines due to the decrease in the D value.

Figure 8 shows a comparison between the TRESR spectrum observed at 300 ns and the simulated spectra calculated at several r distances. The spectrum at the maximized distance of 0.644 nm has two main lines with A/E polarization, the splitting of which is 10 mT which coincides with that between the outer humps of the observed spectrum. However, there is no strong signal in the central part of the spectrum, which is different from the observed one. At $r=0.720$ nm, the simulated spectrum has A/E polarization with two humps at both wing sides of the spectrum, but does not reproduce the observed one totally. On the other hand, in the case of more than 1.0 nm, the simulated spectrum reproduces the strong A/E-polarized signals at the central part of the observed one as shown in Fig. 8(d), while no clear signals are seen in the wings of the spectrum, which correspond to the broad component in the observed spectrum. Consequently, there is no simulated spectrum that satisfactorily reproduced the overall shape and width of the observed one. A reasonable agreement between simulation and experiment was not obtained even in calculating with any other parameter combinations of J_1, t, and r. In our previous paper,[23] we simulated only the sharp component in the observed spectrum using a single set of parameters. The lifetime broadening of each resonance line[55] did not help in simulating the observed spectrum. The inaccessibility of the simulation with any single parameter sets relative to the observed spectrum indicates that the hole produced from a photoinduced electron transfer of the CT complex does not exist at a specific distance separated from the electron-acceptor molecules in the amorphous PVCz film. Generally, trap sites, which can have irregular molecular structures, are scatteringly situated in amorphous solids. Hence, we take into account the distribution of e-h separation distances. Such considerations lead to the conclusion that the e-h pairs having short and middle distances of less than 0.9 nm mainly provide the broad component in the observed spectrum, and that the long distant e-h pairs with separations of more than 0.9 nm give rise to the observed sharp component.

Here we introduce the distribution function of $g(r)$ representing the probability density that a hole exists at a distance r from an electron. In order to simulate the observed spectrum, the S_{ran} function multiplied by $g(r)$ has to be integrated from r_1 to infinity, about r in the spherical polar coordinate,

$$S_{eh}(t) = \int_{r_1}^{\infty} S_{ran}(t,r)g(r)r^2 dr. \tag{10}$$

Although S_{ran} is a function of t, ω_e, ω_h, J, and D in Eq. (7), we now can rearrange it to a function of t and r because the J and D values were approximated as a function of r and the other parameters were fixed or optimized in the discussion above. Figure 9(a) demonstrates a simulated spectrum that assumes a uniform distribution for $g(r)$ as shown in Fig. 9(d). In this spectrum, we can see both sharp and broad components. However, the sharp component due to the long-distant e-h pairs is excessively strengthened, compared with the observed spectrum. This fact excludes a large population of the long-distant e-h pairs generated by long-range hole transfer. On the other hand, the simulations using distribution functions of exponential, Poisson, Gaussian, and asymmetric triangle, which depress the population of the long-distant e-h pairs, as illustrated in Fig. 9(e), show fairly good agreement with the spectrum observed at 300 ns. The simulations with these monotone decreasing-distribution functions, however, have a tendency for the relative intensity of the broad component, due to short-distant e-h pairs to be slightly larger than the observed one.

In order to correct the misfit between simulation and experiment, we next introduce a separation-distance-dependent recombination of the trapped e-h pairs. If the recombination occurs by the escape of a hole from a trap site and the hole

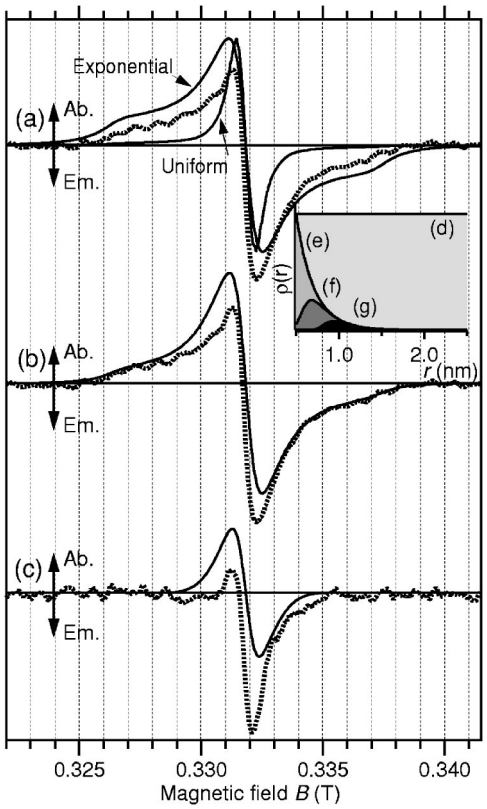

FIG. 9. *X*-band simulation spectra for the trapped e-h pair in the TCNB-doped PVCz film (a), (b), and (c) taking into account the distributions of the separation distance (d), (e), (f), and (g). The simulations of (a), (b), and (c) are obtained by using the distribution functions of (d) and (e), (f), and (g) in the inset, respectively. The parameters employed for the calculation of the component spectra at various distances are the same as those in Fig. 7. The parameters used in determining the exponential distribution are the following: r_e=0.21 nm, $k_1=1\times10^7\ s^{-1}$, and $\beta=1.0\times10^1\ \mathrm{nm}^{-1}$. The spectra denoted by the dotted lines in (a), (b), and (c) are the spectra observed at 0.3, 0.3, and 4.0 μs, respectively.

hops among the nearest-neighboring Cz units (diffusion), the detrapping assisted by thermal energy must be a rate-determinant step, because the hopping rate is of the order of a few ns. However, it is improper for the detrapping process to depend on the r distance. Therefore, such a multistep process in which the rate is determined by detrapping seems to be unsuitable for the r dependence, and it is quite reasonable to assume a single-step recombination such as a tunneling or superexchange mechanism. The rate constant of this step can usually be expressed by the next exponential function,

$$k_{\mathrm{rec}}(r;k,\beta)=k_1\exp[-\beta(r-r_1)], \tag{11}$$

where k_1 and β are parameters. Taking a normalized exponential distribution with an exponent of $1/r_e$ as the initial distribution immediately after photoexcitation and the recombination rate constant represented by Eq. (11), the time-dependent distribution function $\rho_d(t,r;r_e,k_1,\beta)$ is simply derived as

$$\begin{aligned}\rho_d(t,r;r_e,k_1,\beta)&=g(r;r_e)\exp[-k_{rec}(r;k_1,\beta)t]\\&=\frac{1}{r_e}\exp\left\{-\frac{r-r_1}{r_e}-k_1\exp[-\beta(r-r_1)]t\right\}.\end{aligned} \tag{12}$$

Because the trapped e-h pairs with short distances have faster recombination-rate constants, the ρ_d function decreases sequentially from the shortest-distant e-h pairs with time. The ESR spectrum of the trapped e-h pairs at time t is redefined using ρ_d,

$$\begin{aligned}S_{eh}(t;r_e,k_1,\beta)&=\int_{r_1}^{\infty}S_{ran}(0,r)\rho_d(t,r;r_e,k_1,\beta)r^2dr\\&=\int_{r_1}^{\infty}S_{ran}(0,r)\frac{r^2}{r_e}\\&\quad\times\exp\left\{-\frac{r-r_1}{r_e}-k_1\exp[-\beta(r-r_1)]t\right\}dr.\end{aligned} \tag{13}$$

Here we may let β be a constant, because it has been estimated to be about 10 nm^{-1} in many cases of single-step charge transfer.[68,69] The k_1 value should be a fitting parameter in the simulation of the spectrum observed at t=300 ns. The initial distribution function ρ_d can be directly determined from the ESR measurements at less than 300 ns, but those were inaccessible due to the time-resolution limit of the spectrometers used and the zero-quantum oscillations in early times. Therefore, the r_e distance that characterizes the exponential distribution was also set as a parameter to be optimized in the simulation.

As shown in Fig. 9(b), the ESR simulation according to Eq. (13) based on the r-dependent recombination weakens the broad component and provides a much better fit than that of a simple exponential distribution, except for the net emissive ST_+ polarization. The optimized k_1 and r_e values are $1\times10^7\ \mathrm{s}^{-1}$ and 0.21 nm, respectively. ρ_d at t=300 ns with the optimized parameters clarified that a majority of the short-distant e-h pairs has been significantly depopulated even at 300 ns, as illustrated in Fig. 9(f). The calculation of ρ_d using the same parameters predicts that further depopulation of the e-h pairs with $r\leqslant0.75$ nm proceeds at t=4 μs. Only approximately 15% in the initial number of the e-h pairs, corresponding to long-distant pairs, has survived at 4 μs [Fig. 9(g)]. In the simulation spectrum of Fig. 9(c), the broad component due to short-distant pairs almost disappears at 4 μs. The spectrum observed at 4 μs is rather distorted from the symmetric shape of pure ST_0 polarization by the relatively strong contribution of the net E polarization, but the spectral width agrees with that of the simulation spectrum, due to long-distant e-h pairs escaping from the single-step recombination up to 4 μs. The observed sharpening of the ESR spectrum at later times is basically understood by the r-dependent single-step recombination of the trapped e-h pairs.

B. ST_+ polarization

We detected not only the multiplet ST_0 polarization, but also the net E polarization due to the ST_+ mixing on the trapped e-h pairs in the PVCz film sample. The J value of the e-h pair causing the ST_+ polarization was estimated to be approximately +4.8 GHz (+0.17 T) from the field dependence of the net E polarization. On the other hand, the J_1 value of the trapped e-h pair is -2.0×10^2 MHz at $r_1=0.5$ nm, which is estimated from simulations of the ST_0 polarization. The sign and size of the J value of the e-h pair providing the ST_+ polarization are different from those of the trapped e-h pairs. The sign and size changes in the J value have been reported in many electron-transfer systems in homogeneous fluid solutions[62–66] and in heterogeneous media.[55,70–72] This phenomenon in homogeneous systems can be interpreted in terms of the CT interaction between the e-h pair and the nearby charge-recombined states.[73–76] Because the spectral simulations of the ST_0 polarization clarified that direct recombination from the e-h pairs to the ground-singlet (S_0) state takes place in the present system, it is reasonable to consider the CT interaction in the exchange interaction of the e-h pairs of TCNB-doped PVCz. The energy difference between the interacting states at the most stable nuclear configuration for the e-h pair is a critical factor in determining the sign as well as the size of the J value due to the CT interaction. The energy of the e-h pair causing the ST_+ polarization should be different from that of the trapped e-h pairs. The state energy of the trapped e-h pairs is expected to be lower than that of the canonical e-h pair that can undergo the usual hole hops, because the trap site where the hole is captured stabilizes the hole energy by a trap depth of more than 25 meV of thermal energy at room temperature (Fig. 10). The e-h pair causing the ST_+ polarization belongs to the canonical e-h pair and should have a higher energy than that of the trapped e-h pairs. Based on this energy difference, it can be assumed that the S_0 state at the same nuclear configuration as the e-h pairs lies between the canonical and the trapped e-h pair states. If the CT interaction between this virtual S_0 state and the S states of the canonical and trapped pairs mainly gives rise to the singlet-triplet splitting of the e-h pairs, such a spin-selective perturbation results in the positive and negative J values in the canonical and trapped pairs, respectively.

The $|J|$ value of +4.8 GHz estimated from the ST_+ polarization is obviously larger than that of the canonical e-h pair, with a long separation distance of $r\geqslant1.0$ nm. Therefore, the canonical e-h pair causing the ST_+ polarization is assigned to the contact or middle-distant e-h pairs with $r<1.0$ nm. These pairs correspond to site 1 and site 2 in the one-dimensional lattice model proposed in the previous papers (cf. a scheme in Fig. 11).[16–18] The simple one-dimensional lattice model can well explain the spin dynamics of the geminate, canonical e-h pair in the PVCz film. Although the PVCz film is an amorphous solid, the one-dimensionality in the model arises from the helically structured Cz ensemble along the methylene polymer chain that tightly binds them in a nanoscale area. In this model, the contact e-h pair has a substantially large J value of more than $+1.0\times10^1$ GHz at site 1. Hence, the e-h pair with a J value of +4.8 GHz may

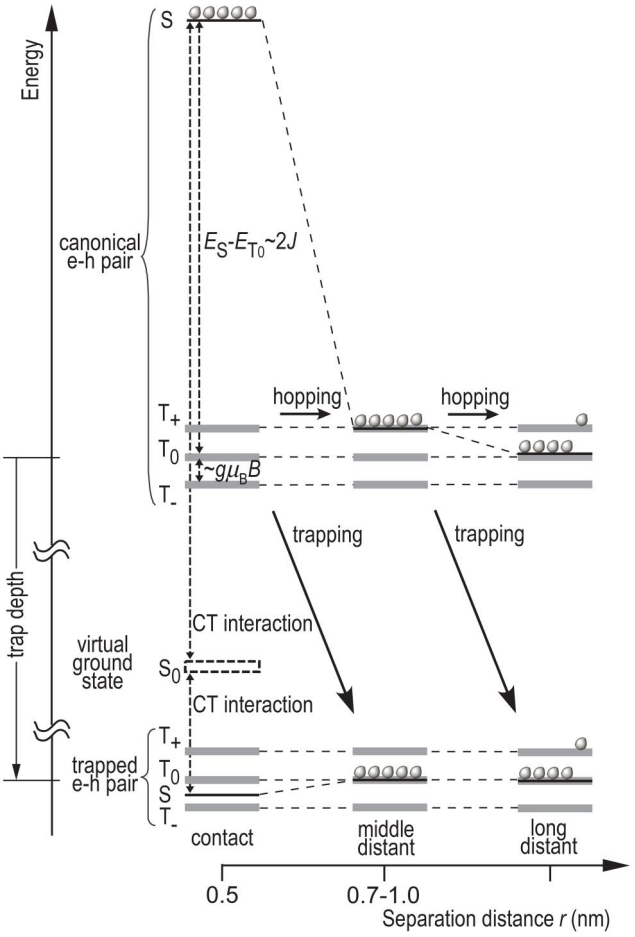

FIG. 10. State-energy diagram of the canonical e-h pair, the virtual S_0 state and the trapped e-h pair captured in a deep-trap site. Circles indicate populations originating from a singlet-born e-h pair. The solid and broken arrows denote the elementary hole dynamics and interactions, respectively.

be the canonical e-h pair at site 2. This is represented by the canonical e-h pair at a middle distance in Fig. 10. In this middle-distant canonical e-h pair of which the S and T_+ states are nearly degenerate in energy, the spin conversion can happen, because the period for a hole to hop toward the next sites in PVCz is estimated to be approximately 2 ns, which is comparable to the time for population transfer between the S and T_+ states driven by hyperfine interaction. Actually, a level-cross mechanism in the spin dynamics of the canonical e-h pair that is equivalent to the ST_+ polarization has been observed, as noted in the previous papers.[16,17] Comparing the observed spectrum and the ST_0-polarization simulation for the trapped e-h pairs in Fig. 9(b) again, it is clear that the ST_+ polarization appears more strongly in the sharp component of the long-distant pairs than in the broad component of the short-distant pairs. The relative contribution of the ST_+ polarization to the long-distant trapped e-h pair became more significant at a later time in Fig. 9(c). Integration of these facts and the discussion of the ST_+-polarization mechanism leads to the conclusion that the long-distant trapped e-h pairs are generated through the middle-distant canonical e-h pair, as shown in Fig. 10. The

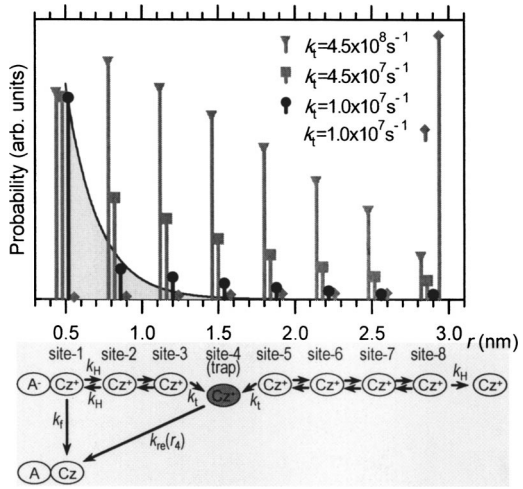

FIG. 11. Experimentally estimated initial spatial distribution of the trapped e-h pairs (shaded graph) and calculated populations in trap sites (stick graphs). The calculations are based on a uniform distribution of the trap site, the kinetics of the stepwise hole hops, and the single-step recombination from the trap sites in the one-dimensional lattice model. The sticks marked by triangles, squares, and circles were calculated under an initial condition in which all holes exist at site 1 at zero time, while the rhomboid sticks were obtained by simulation of the kinetics beginning at site 8. The distance between each neighboring Cz unit in the lattice is approximated to be 0.34 nm.

dynamics from the short-distant pairs with $r<1$ nm to the long-distant ones supports the presence of the stepwise hole hops, rather than the long-range hole jump of 2–3 nm due to thermalization or autoionization, which is derived from a premise in the Onsager theory.

C. Distribution

The ST_0-polarized spectra of the trapped e-h pairs, which have more structures than the ST_+-polarized one, were fairly well simulated by introducing the distributions of separation distance and the distance-dependent recombination rate. The distribution functions were represented by the monotone decreasing functions such as the exponential, Poisson, Gaussian, and asymmetric triangle. The initial distribution of trapped e-h pairs estimated from the simulation of the observed spectra is illustrated in Fig. 11. The observation of ST_+ polarization on the long-distant e-h pairs elucidated that the initial distribution of separation distance is associated with the stepwise hole hops in the geminate e-h pair, but does not reflect the hole-transfer distance distribution in the first step. The r distribution of the canonical e-h pair in PVCz molecular solids has been calculated in the way in which the hole hop is treated as a stochastic process by several authors.[77–80] In this section, therefore, we discuss the tailing property in the obtained spatial distribution of the trapped e-h pair by means of a deterministic simulation using rate equations based on the simple one-dimensional lattice including trap sites.

In the previous studies, we have clarified that the one-dimensional lattice model with seven or eight sites (Fig. 11) properly represents the dynamics of the geminate canonical e-h pair. Furthermore, in this work, we modified this model by introducing trap sites. For example, the scheme illustrates the case in which site 4 serves as a trap site from where the hole cannot return to the canonical sites, but can directly recombine to the S_0 state. The kinetic equations for the one-dimensional lattice model with a trap site at site t can be expressed using density operators (ρ) as follows:

$$\begin{cases} \rho_0' = +k_f\rho_1 + k_{re}(r_t)\rho_t, \\ \rho_1' = -k_H\rho_1 + k_H\rho_2 - k_f\rho_1, \\ \rho_2' = -k_H\rho_2 - k_H\rho_2 + k_H\rho_1 + k_H\rho_3, \\ \quad\vdots \\ \rho_{t-1}' = -k_H\rho_{t-1} - k_t\rho_{t-1} + k_H\rho_{t-2}, \\ \rho_t' = +k_t\rho_{t-1} + k_t\rho_{t+1} - k_{re}(r_t)\rho_t, \\ \rho_{t+1}' = -k_H\rho_{t+1} - k_t\rho_{t+1} + k_H\rho_{t+2}, \\ \quad\vdots \\ \rho_8' = -k_H\rho_8 - k_H\rho_8 + k_H\rho_7, \\ \rho_9' = +k_H\rho_8. \end{cases} \tag{14}$$

k_f and k_H, which are the rate constants of recombination from the contact e-h pair at site 1 and of hole hopping, have already been estimated to be 7.0×10^7 and 4.5×10^8 s^{-1}, respectively. However, the trapping-rate constant of k_t is an unknown rate constant. The population in trap site t at time t_0 is obtained from the $\rho_t(t_0)$ of the kinetic equations. Thus we numerically solve the simultaneous differential equations employing various k_t values. Because the trap site can be thought to uniformly exist in the amorphous film, we can also set the probabilities of trap sites in the one-dimensional lattice model to be equal to p_t at any position. The population in the trap site at site i (P_i) caused by the geminate pair dynamics can be defined by

$$P_i(t_0) = \sum_{l=1}^{8}\sum_{m=1}^{{}_8C_l} (p_t)^l \rho_i^{l,m}(t_0) \simeq \sum_{m=1}^{8} p_t \rho_i^{1,m}(t_0). \tag{15}$$

Because the probability of trap sites is quite low ($p_t \ll 1$), the higher-order terms with $l \geqslant 2$, which describe the case where there is simultaneously more than one trap site in the same lattice, can be ignored. Let t_0 be 30 ns for this system, because the transient photocurrent measurements on the TCNB-doped PVCz film indicate that the dynamics of the geminate canonical e-h pair is almost completed at 30 ns.[17]

The population distribution of the hole in trap sites at various positions calculated with an initial condition of $\rho_1(0)=1$ and $\rho_{i\neq1}(0)=0$ is shown in Fig. 11. In the case of $k_t=k_H$, the population at site 2 is maximum, and relatively large populations are recognized at the long-distant sites. These properties are different from the initial distribution of the trapped e-h pairs estimated from the experiments. When the k_t value is made smaller than k_H, the population in the long-distant sites decreases. The population distribution calculated using $k_t=1\times10^7$ s^{-1} satisfactorily reproduces the experimental distribution, having a rapid decay in the short-distance region and a slow decrease in the long-distance

region. The fact that k_H is much greater than k_t, which is a rate constant for exothermic trapping, suggests a contribution of resonance interaction in the hole hops among the Cz units. Next, for comparison with the long-range jumping of a hole, we calculated the population distribution under the condition of $\rho_8(0)=1$ and $\rho_{i\neq 8}(0)=0$. The population is maximum at site 8, and no significant population is present in the short range, which is completely different from the experiments. The kinetic simulation of the distribution also leads to the conclusion that the stepwise hole hops are the dominant dynamics in the photocarrier generation in the molecular solid of PVCz.

Finally, the energetic distribution of the trap site should be noted because the PVCz film is not a homogeneous molecular solid. The trap site should also be distributed in energy space. However, we could apparently understand the spin polarizations and the spatial distribution of the trapped e-h pairs by taking into account the trap sites with a single deep level which is uniformly distributed in real space. It seems unnatural that there are only two kinds of e-h pairs, the canonical and deep-trapped sites. This is interpreted in terms of easy release of a hole from shallow traps at room temperature. If the hole can quickly leave a trap site even though the hole drops into the trap, such a trap site can be regarded to be the same as the canonical sites. Hence, only deep-trap sites from which the hole can barely escape after trapping function as a trap site. This may be the reason why the one-dimensional model using only canonical and trapped e-h pairs consistently explains the experimental data obtained at room temperature. Nevertheless, if the e-h pairs cannot escape from the shallow-trap sites by lowering the temperature and live long enough to be detected by ESR, the presence of the distribution of the trap depth would be clearly reflected in the spin polarization and/or the spectral shape. Because the exchange interaction of the e-h pairs in the TCNB-doped PVCz film is dominated by the CT interaction, the trap-depth distribution relates to the distribution of the J value. The possibility of the J distribution clearly needs further investigation. The TRESR experiments at various temperatures will allow us to clarify the energetic distribution of trap sites.

V. CONCLUSIONS

We have observed the spin-polarized ESR spectra of the e-h pairs captured in deep-trap sites. The trapped e-h pair had multiplet A/E-and net E-polarizations. Based on the multifrequency ESR experiments, it was clarified that the multiplet and net polarizations arise from ST_0 mixing in the trapped pairs and ST_+ mixing in the canonical pairs, respectively. The phases of the ST_0 and ST_+ polarizations indicated that the canonical and trapped pairs have a positive and negative J value, respectively. The sign difference of the J value is interpreted in terms of the CT interaction with the virtual S_0 state located in energy between the canonical and trapped pairs. The ST_0 polarization of the observed spectra could not be simulated by any single magnetic-parameter set. However, the simulation accounting for the distribution of the e-h pair separation distance on a nanometer scale and the distance-dependent recombination to the S_0 state reproduced well the observed spectra that were comprised of broad and sharp components. The ST_+ polarization and the initial-separation-distance distribution of the trapped pairs indicate that the initial charge separation in the PVCz film happens through stepwise hole hops in the one-dimensional lattice model, rather than the single-step long-range hole jump. The distant-dependent rate constant with respect to the recombination, on the other hand, suggests that the recombination from the trapped pairs is achieved by single-step tunneling in contrast to the charge-separation process.

ACKNOWLEDGMENTS

Thanks are due to Professor S. Yamauchi (Tohoku University) and Dr. Y. Iwasaki (Osaka University) for TRESR measurements at the W band. T.I. appreciates Professor P. J. Hore (Oxford University) for his fruitful discussions about spin-correlated radical pairs. This research was funded in part by a Grant-in-Aid for Scientific Research (Grant No. 15310069) from the Japan Ministry of Education, Culture, Sports, Science, and Technology (MEXT) of the Japanese Government, and the Murata Science Foundation. A part of the calculated results in this research was obtained using supercomputing resources at the Information Synergy Center, Tohoku University.

*Corresponding author. Electronic address: ikoma@tagen.tohoku.ac.jp

[1] L. Onsager, Phys. Rev. **54**, 554 (1938).
[2] P. J. Melz, J. Chem. Phys. **57**, 1694 (1972).
[3] Y. Wang, Nature (London) **356**, 585 (1992).
[4] J. M. Peason and M. Stolka, *Poly(N-vinylcarbazole)* (Gordon and Breach, New York, 1981).
[5] M. Yokoyama, Y. Endo, and H. Mikawa, Bull. Chem. Soc. Jpn. **49**, 1538 (1976).
[6] M. Yokoyama, Y. Endo, A. Matsubara, and H. Mikawa, J. Chem. Phys. **75**, 3006 (1981).
[7] M. Yokoyama, S. Shimokihara, A. Matsubara, and H. Mikawa, J. Chem. Phys. **76**, 724 (1982).
[8] M. Yokoyama, S. Shimokihara, A. Matsubara, and H. Mikawa, Polym. J. (Tokyo, Jpn.) **14**, 77 (1982).
[9] M. Yokoyama and H. Mikawa, Photograph. Sci. Eng. **26**, 143 (1982).
[10] K. Okamoto and A. Itaya, Bull. Chem. Soc. Jpn. **57**, 1626 (1984).
[11] E. A. Silinsh and V. Čápek, *Organic Molecular Crystals. Interaction, Localization and Transport Phenomena* (American Institute of Physics, New York, 1994).
[12] J. Noolandi and K. M. Hong, J. Chem. Phys. **70**, 3230 (1979).
[13] L. Sebastian, G. Weiser, G. Peter, and H. Bässler, Chem. Phys. **75**, 103 (1982).
[14] H. Miysaka, T. Moriyama, S. Kotani, R. Muneyasu, and A. Itaya, Chem. Phys. Lett. **225**, 315 (1994).

[15] H. Miyasaka, T. Moriyama, T. Ide, and A. Itaya, Chem. Phys. Lett. **292**, 339 (1998).
[16] F. Ito, T. Ikoma, K. Akiyama, Y. Kobori, and S. Tero-Kubota, J. Am. Chem. Soc. **125**, 4722 (2003).
[17] F. Ito, T. Ikoma, K. Akiyama, S. Tero-Kubota, and A. Watanabe, J. Phys. Chem. B **109**, 8707 (2005).
[18] F. Ito, T. Ikoma, K. Akiyama, and S. Tero-Kubota, J. Phys. Chem. B **109**, 7208 (2005).
[19] A. Carrington and A. D. McLachlan, *Introduction to Magnetic Resonance* (Harper and Row, New York, 1967).
[20] N. M. Atherton, *Principles of Electron Spin Resonance* (Ellis Horwood, London, 1993).
[21] P. J. Hore, in *Advanced EPR. Applications in Biology and Biochemistry*, edited by A. J. Hoff (Elsevier, Amsterdam, 1989), p. 405.
[22] A. Angerhofer and R. Bittl, Photochem. Photobiol. **63**, 11 (1996).
[23] T. Ikoma, M. Nakai, K. Akiyama, S. Tero-Kubota, and T. Ishii, Angew. Chem., Int. Ed. **40**, 3234 (2001).
[24] K. M. Salikhov, Y. N. Molin, R. Z. Sagdeev, and A. L. Buchachenko, *Spin Polarization and Magnetic Effects in Radical Reactions* (Elsevier, Amsterdam, 1984).
[25] L. T. Muus, P. W. Atkins, K. A. McLauchlan, and J. B. Pedersen, *Chemically Induced Magnetic Polarization, Theory, Technique, and Applications* (D. Reidel, Dordrecht, 1977).
[26] J. H. Freed and J. B. Pedersen, in *Advances in Magnetic Resonance 8*, edited by J. S. Waugh (Academic Press, London, 1976).
[27] I. A. Shkrob and A. D. Trifunac, Phys. Rev. B **54**, 15073 (1996).
[28] I. A. Shkrob and A. D. Trifunac, J. Chem. Phys. **107**, 2374 (1997).
[29] H. Hayashi, *Introduction to Dynamic Spin Chemistry, Magnetic Field Effects on Chemical and Biochemical Reactions* (World Scientific, Singapore, 2004).
[30] K. A. McLauchlan, in *Modern Pulsed and Continuous-wave Electron Spin Resonance*, edited by L. Kevan and M. K. Bowman (John Wiley & Sons, New York, 1990).
[31] F. Kieffer, C. Meyer, and J. Rigaut, Chem. Phys. Lett. **11**, 359 (1971).
[32] F. Kieffer, C. Lapersonne-Meyer, and J. Rigaut, Int. J. Radiat. Phys. Chem. **6**, 79 (1974).
[33] K. I. Zamaraev and R. F. Khairutdinov, Chem. Phys. **4**, 181 (1974).
[34] M. Tachiya and A. Mozumder, Chem. Phys. Lett. **28**, 87 (1974).
[35] F. S. Dainton, M. J. Pilling, and S. A. Rice, J. Chem. Soc., Faraday Trans. 2 **71**, 1311 (1975).
[36] M. J. Pilling and S. A. Rice, J. Phys. Chem. **79**, 3035 (1975).
[37] Y. Hama, Y. Kimura, M. Tsumura, and N. Omi, Chem. Phys. **53**, 115 (1980).
[38] H. Ohkita, W. Sakai, A. Tsuchida, and M. Yamamoto, Macromolecules **30**, 5376 (1997).
[39] H. Ohkita, W. Sakai, A. Tsuchida, and M. Yamamoto, J. Phys. Chem. **101**, 10241 (1997).
[40] T. Ikoma, K. Akiyama, S. Tero-Kubota, and Y. Ikegami, J. Phys. Chem. **95**, 7119 (1991).
[41] T. Ehara, K. Akiyama, T. Ikoma, Y. Ikegami, and S. Tero-Kubota, J. Phys. Chem. **99**, 2292 (1995).
[42] T. Ikoma, K. Akiyama, S. Tero-Kubota, and Y. Ikegami, J. Chem. Soc., Faraday Trans. **94**, 1197 (1998).
[43] Y. Nagano, T. Ikoma, K. Akiyama, and S. Tero-Kubota, J. Chem. Phys. **114**, 1775 (2001).
[44] T. Shimokage. T. Ikoma, K. Akiyama, and S. Tero-Kubota, Spectrochim. Acta, Part A **58**, 1201 (2002).
[45] A. Katsuki, K. Akiyama, Y. Ikegami, and T. Tero-Kubota, J. Am. Chem. Soc. **116**, 12065 (1994).
[46] S. Sasaki, A. Katsuki, K. Akiyama, and S. Tero-Kubota, J. Am. Chem. Soc. **119**, 1323 (1997).
[47] S. Sasaki, Y. Kobori, K. Akiyama, and S. Tero-Kubota, J. Phys. Chem. **102**, 8078 (1998).
[48] S. Tero-Kubota, A. Katsuki, and Y. Kobori, J. Photochem. Photobiol. C **2**, 17 (2001).
[49] T. Tachikawa, Y. Kobori, K. Akiyama, A. Katsuki, Y. Usui, U. E. Steiner, and S. Tero-Kubota, Mol. Phys. **100**, 1413 (2002).
[50] T. Tachikawa, Y. Kobori, K. Akiyama, A. Katsuki, U. E. Steiner, and S. Tero-Kubota, Chem. Phys. Lett. **360**, 13 (2002).
[51] K. Hasharoni, H. Levanon, J. v. Gersdorff, H. Kurreck, and K. Möbius, J. Chem. Phys. **98**, 2916 (1993).
[52] J. Schlüpmann, F. Lendzian, M. Plato, and K. Möbius, J. Chem. Soc., Faraday Trans. **89**, 2853 (1993).
[53] L. Franco, L. Pasimeni, G. Ponterini, M. Ruzzi, and U. Segre, Phys. Chem. Chem. Phys. **3**, 1736 (2001).
[54] U. Till and P. J. Hore, Mol. Phys. **90**, 289 (1997).
[55] U. Till, I. B. Klenina, I. I. Proskuryakov, A. J. Hoff, and P. J. Hore, J. Phys. Chem. B **101**, 10939 (1997).
[56] F. J. J. de Kanter, J. H. den Hollander, A. H. Huizer, R. Kaptein, Mol. Phys. **34**, 857 (1977).
[57] I. A. Shkrob, Chem. Phys. Lett. **264**, 417 (1997).
[58] K. Maeda, N. Suzuki, and T. Azumi, J. Phys. Chem. **97**, 9562 (1993).
[59] T. Aizawa, T. Sakata, S. Itoh, K. Maeda, and T. Azumi, Chem. Phys. Lett. **195**, 16 (1992).
[60] H. Cao, Y. Fujiwara, T. Haino, Y. Fukazawa, C. Tung, and Y. Tanimoto, Bull. Chem. Soc. Jpn. **69**, 2801 (1996).
[61] F. J. J. de Kanter and R. Kaptein, J. Am. Chem. Soc. **104**, 4759 (1982).
[62] S. Sekiguchi, K. Akiyama, S. Tero-Kubota, Chem. Phys. Lett. **263**. 161 (1996).
[63] S. Sekiguchi, Y. Kobori, K. Akiyama, and S. Tero-Kubota, J. Am. Chem. Soc. **120**, 1325 (1998).
[64] Y. Kobori, S. Sekiguchi, K. Akiyama, and S. Tero-Kubota, J. Phys. Chem. A **103**, 5416 (1999).
[65] Y. Kobori, K. Akiyama, and S. Tero-Kubota, J. Chem. Phys. **113**, 465 (2000).
[66] S. Tero-Kubota, Pure Appl. Chem. **73**, 519 (2001).
[67] A. Carrington and A. D. McLachlan, *Introduction to Magnetic Resonance* (Harper and Row, New York, 1967), p. 117.
[68] M. Tachiya and A. Mozumder, Chem. Phys. Lett. **34**, 77 (1975).
[69] S. Murata and M. Tachiya, J. Phys. Chem. **100**, 4064 (1996).
[70] P. J. Hore, D. J. Riley, J. J. Semlyen, G. Zwanenburg, and A. J. Hoff, Biochim. Biophys. Acta **1141**, 221 (1993).
[71] M. K. Bosch, P. Gast, E. M. Franken, G. Zwanenburg, P. J. Hore, and A. J. Hoff, Biochim. Biophys. Acta **1276**, 106 (1996).
[72] R. van der Vos, E. M. Franken, S. J. Sexton, S. Shochat, P. Gast, P. J. Hore, and A. J. Hoff, Biochim. Biophys. Acta **1230**, 51 (1995).
[73] Y. Kobori, T. Yago, K. Akiyama, and S. Tero-Kubota, J. Am. Chem. Soc. **123**, 9722 (2001).
[74] T. Yago, Y. Kobori, K. Akiyama, and S. Tero-Kubota, J. Phys. Chem. B **106**, 10074 (2002).
[75] S. Tero-Kubota, K. Zikihara, T. Yago, Y. Kobori, and K. Akiyama, Appl. Magn. Reson. **26**, 145 (2004).

[76] A. Sekihara, H. Honma, T. Fukuju, K. Maeda, and H. Murai, Res. Chem. Intermed. **24**, 859 (1998).
[77] S. Kotani, H. Miyasaka, and A. Itaya, J. Phys. Chem. **100**, 19898 (1996).
[78] K. Watanabe, T. Asahi, and H. Masuhara, J. Phys. Chem. **100**, 18436 (1996).
[79] K. Watanabe, T. Asahi, and H. Masuhara, J. Phys. Chem. B **101**, 5131 (1997).
[80] D. Abramavicius, V. Gulbians, and L. Valkunas, Synth. Met. **109**, 39 (2000).